

Studies of nonresonant Higgs pair production at electron-proton colliders

Adil Jueid, Jinheung Kim, Soojin Lee, Jeonghyeon Song

Department of Physics, Konkuk University, Seoul 05029, Republic of Korea

Abstract

The measurement of the Higgs quartic coupling modifier between a Higgs boson pair and a vector boson pair, κ_{2V} , is expected to be achieved from vector-boson fusion (VBF) production of a Higgs boson pair. However, this process involves another unmeasured parameter, the trilinear Higgs self-coupling modifier κ_λ . A sensitivity analysis should target both parameters. Since the LHC cannot avoid the gluon fusion pollution, which becomes severe for non-SM κ_λ , an electron-proton collider is more appropriate for the comprehensive measurement. In this regard, we study the VBF production of a Higgs boson pair in the $b\bar{b}b\bar{b}$ final state at the LHeC and FCC-he. Performing detailed analysis using the simulated dataset, we devise the search strategy specialized at the LHeC and FCC-he and give a prediction for the sensitivity to both κ_{2V} and κ_λ . We find that the two electron-proton colliders have high potential: the LHeC has similar exclusion prospects as the HL-LHC; the FCC-he is extremely efficient, excluding the parameter space outside $\kappa_{2V} \in [0.8, 1.2]$ and $\kappa_\lambda \in [1, 2.5]$ at 95% C.L. for the total luminosity of 10 ab^{-1} and 10% uncertainty on the background yields.

Keywords: $HHVV$ coupling, trilinear Higgs self-coupling, LHeC, FCC-he

1. Introduction

Albeit the absence of any signatures of the physics beyond the Standard Model (BSM), the journey to the final theory of the Universe will never stop. One important task to achieve the goal is to measure every coupling among the SM particles precisely, especially to the Higgs boson H . The Higgs coupling modifiers associated with a single Higgs boson have been observed to be SM-like at the LHC [1, 2]. Their future projections at the high luminosity LHC (HL-LHC) expect the precisions at or below the percent level [3]. However, coupling modifiers involving a pair of Higgs bosons remain unmeasured, such as κ_λ for the trilinear Higgs self-coupling and κ_{2V} for the quartic coupling between a Higgs boson pair and a vector boson pair. The κ_λ shall be probed mainly from nonresonant Higgs boson pair (HH) production via gluon fusion: the triangle diagram mediated by the Higgs boson in the s -channel gives access to κ_λ . It is found that if $\kappa_\lambda \neq 1$, non-trivial changes occur on both the shape and rate of the main kinematic distributions [4]. The current observed interval at the 95% confidence level (C.L.) is $-5.0 < \kappa_\lambda < 12.0$ in the ATLAS analysis [5] and $-11.8 < \kappa_\lambda < 18.8$ in the CMS analysis [6]. Several studies of the prospects for measuring κ_λ at the HL-LHC and future colliders have been performed [7, 8, 9, 10, 11, 12, 13, 14], which expect more stringent bounds.

The quartic coupling modifier κ_{2V} is much more challenging to measure at the LHC since the most efficient process, non-resonant HH production via vector boson fusion (VBF), has

very small cross-section of $\sigma_{\text{VBF}}^{\text{SM}}(pp \rightarrow HHjj)|_{\text{N}^3\text{LO}} = 1.73 \text{ fb}$ at $\sqrt{s} = 13 \text{ TeV}$ [15] in addition to the huge SM backgrounds. The ATLAS collaboration performed the first search and excluded $\kappa_{2V} < -0.76$ and $\kappa_{2V} > 2.90$ at the 95% C.L. for $\kappa_V = 1$ and $\kappa_\lambda = 1$ [16]. The assumption of $\kappa_V = 1$ is well motivated by the Higgs precision measurements at the LHC, but $\kappa_\lambda = 1$ is questionable. The VBF production of HH , which also depends on κ_λ via the H -mediated s -channel diagram, is susceptible to anomalous Higgs self-coupling ($\kappa_\lambda \neq 1$). For example, the cross-section for $\kappa_\lambda = 5$ at the 14 TeV LHC is about twenty times that for $\kappa_\lambda = 1$. More serious is the pollution from the gluon fusion production of HH associated with two jets, $gg \rightarrow HHjj$ [17, 18]. This pollution also has the contribution from κ_λ and greatly increases for $\kappa_\lambda \neq 1$.¹ Considering huge QCD uncertainties in the gluon fusion pollution [19], we expect an inevitable limitation to the precision measurement of κ_{2V} at the LHC.

Targeting the measurements of κ_λ and κ_{2V} without the assumption about κ_λ and thus the ambiguity of the gluon fusion pollution, we turn to two electron-proton colliders, the Large Hadron electron Collider (LHeC) [20, 21, 22] and the Future Circular Collider (FCC-he) [23]. The development of the energy recovery linac for the electron beam makes it possible to simultaneously operate the pp and e^-p collisions. In particular, the LHeC has a bright outlook as its working group recently announced the default configuration and staging based on the cost estimation [22]. We find the following advantages of electron-proton colliders in probing rare BSM events:

Email addresses: adil.hep@gmail.com (Adil Jueid), jinheung.kim1216@gmail.com (Jinheung Kim), soojinlee957@gmail.com (Soojin Lee), jhsong@konkuk.ac.kr (Jeonghyeon Song)

¹The ATLAS collaboration treated the gluon fusion pollution as a background because they assumed $\kappa_\lambda = 1$ and thus knew its rate [16].

- The pileup, which degrades the quality of the data for physics analyses, is very small even at the high luminosity option ($\sim 10^{34}/\text{cm}^2/\text{s}$): one expects about 0.1 (1) pileup collisions per event at the LHeC (FCC-he) while $\gtrsim 150$ at the LHC.
- The QCD backgrounds and the higher-order corrections are suppressed, providing a clean environment.
- The charged-current (CC) and neutral-current (NC) processes can be disentangled by tagging the outgoing neutrino (as large missing transverse energy) or electron. Independent measurements of κ_{2W} and κ_{2Z} are possible.
- The asymmetric initial state allows us to distinguish the forward and backward directions, which can increase the signal significance.
- High polarization of the electron beam, P_e , is feasible, as large as $\pm 80\%$ [22]. The CC production cross-section increases by the factor of $(1-P_e)$, while the NC cross-section does not change much.

For the configurations of

$$\begin{aligned} \text{LHeC: } & E_e = 50 \text{ GeV}, \quad E_p = 7 \text{ TeV}, \\ \text{FCC-he: } & E_e = 60 \text{ GeV}, \quad E_p = 50 \text{ TeV}, \end{aligned} \quad (1)$$

we shall analyze the sensitivity of the LHeC and FCC-he to κ_{2V} and κ_λ via the VBF production of HH through the CC channel.² Taking full advantage of the characteristics of the electron-proton collider, we shall propose a search strategy which we believe is optimal for measuring κ_{2V} and κ_λ . Finally, we will present the 95% C.L. exclusion in the $(\kappa_{2V}, \kappa_\lambda)$ space, based on the detector-level analysis of the signals and the relevant backgrounds. The remainder of this letter is organized as follows. In section 2, we discuss the formalism of Higgs boson pair production in e^-p collisions within the κ -framework along with a discussion of the modeling of the signal and background processes. In section 3, we discuss the analysis strategy and present our results. We conclude in section 4.

2. Formalism and modeling for the signal and backgrounds

Based on the observed Higgs precision data via single Higgs production at the LHC, we assume that all the couplings to a *single* Higgs boson are the same as in the SM:

$$\kappa_{Hij} = 1, \quad (2)$$

where i and j are the SM particles. For renormalizable couplings to a Higgs boson pair, we consider

$$\mathcal{L} \supset \kappa_{2V} \frac{g^2}{4} W^{+\mu} W_{\mu}^- H^2 - \kappa_\lambda \frac{3m_H^2}{v} H^3, \quad (3)$$

²In the literature, the e^-p collider phenomenologies of anomalous Higgs couplings associated with a Higgs boson pair were studied in the effective Lagrangian model, via the CC [24] and NC process [25].

where $v \simeq 246$ GeV. Note that κ_{2V} and κ_λ parameterize the BSM interactions within the context of the non-linear effective field theory given by the electroweak chiral Lagrangian [26, 27, 28, 29, 30]³.

Aiming at the precision measurement of κ_{2V} and κ_λ together, we focus on the pair production of Higgs bosons through the CC VBF interaction in the $b\bar{b}b\bar{b}$ final state,

$$pe^- \rightarrow HH + j_f \nu_e \rightarrow b\bar{b}b\bar{b} + j_f \nu_e, \quad (4)$$

where j_f is a forward jet. There are three kinds of Feynman diagrams for this process, the contact one involving HHW^+W^- coupling, the s -channel involving HHH coupling, and the t, u -channels with the square of HW^+W^- coupling. The scattering amplitudes of $W^+W^- \rightarrow HH$ help us to understand the characteristics of the signal. As explicitly shown in Ref. [36], the longitudinally polarized W_L^+ and W_L^- make an overwhelmingly dominant contribution. The corresponding amplitude, \mathcal{M}_{LL} , in the limit of $\sqrt{s} \gg m_H$ satisfies

$$\begin{aligned} \frac{1}{g^2} \mathcal{M}_{LL} = & (\kappa_{2V} - \kappa_V^2) \frac{s}{4m_W^2} + \kappa_\lambda \frac{3m_H^2}{4m_W^2} \\ & + \kappa_V^2 \left[1 - \frac{m_H^2}{2m_W^2} - \frac{2}{\sin^2 \theta^*} \right] - \frac{\kappa_{2V}}{2} + \mathcal{O}\left(\frac{m_{W,H}^2}{s}\right), \end{aligned} \quad (5)$$

where we keep the notation of κ_V to show its effects and θ^* is the scattering angle in the center-of-mass frame of W^+W^- . Note that the effect of κ_λ dominates in the small $m_{HH}(= \sqrt{s})$ region while that of κ_{2V} does in the high m_{HH} region.

First, at the parton level, we calculate the total cross-sections of the signal by varying both κ_{2V} and κ_λ . The calculations have been performed at leading order (LO) using MadGraph_aMC@NLO with a modified UFO [37] model file for the Lagrangian in Eq. (3). Based on the current experimental bounds, we consider $-1 \leq \kappa_{2V} \leq 3$ [16] and $-6 \leq \kappa_\lambda \leq 12$ [5, 6]. The SM cross-section of the process $pe^- \rightarrow HH j_f \nu_e$ is very small: with the unpolarized electron beam, it is $\sigma_{\text{SM}} = 5.97$ ab at the LHeC and $\sigma_{\text{SM}} = 233.77$ ab at the FCC-he. Despite tiny SM signals, it is promising that the total cross-section rapidly increases when either κ_{2V} or κ_λ deviates from their SM values: the two electron-proton colliders can exclude a large portion of the parameter space $(\kappa_{2V}, \kappa_\lambda)$. To show this behavior, we present $\sigma/\sigma_{\text{SM}}$ in Fig. 1. It is clear to see that the deviation from $\kappa_{2V} = 1$ greatly increases the cross-section because it invalidates the cancellation of the longitudinal polarization enhancement, the first term of Eq. (5). The hypothesis of $\kappa_\lambda \neq 1$ also increases the signal cross-section, though less than that of $\kappa_{2V} \neq 1$. Quantitatively, we have a tenfold increase of $\sigma/\sigma_{\text{SM}}$ if $|\kappa_{2V} - 1| = |\kappa_\lambda - 1| = 1$. We also note that the same-sign κ_{2V} and κ_λ yield constructive interference, explaining the negative slopes of the $\sigma/\sigma_{\text{SM}}$ contours: see the first two terms of Eq. (5). In detail, the LHeC and FCC-he show different shapes

³Note that concrete BSM scenarios can accommodate large values of κ_λ at the quantum level [31, 32, 33, 34, 35]. However, it is not straightforward to construct a BSM model that can have a large κ_{2V} without significantly affecting κ_V .

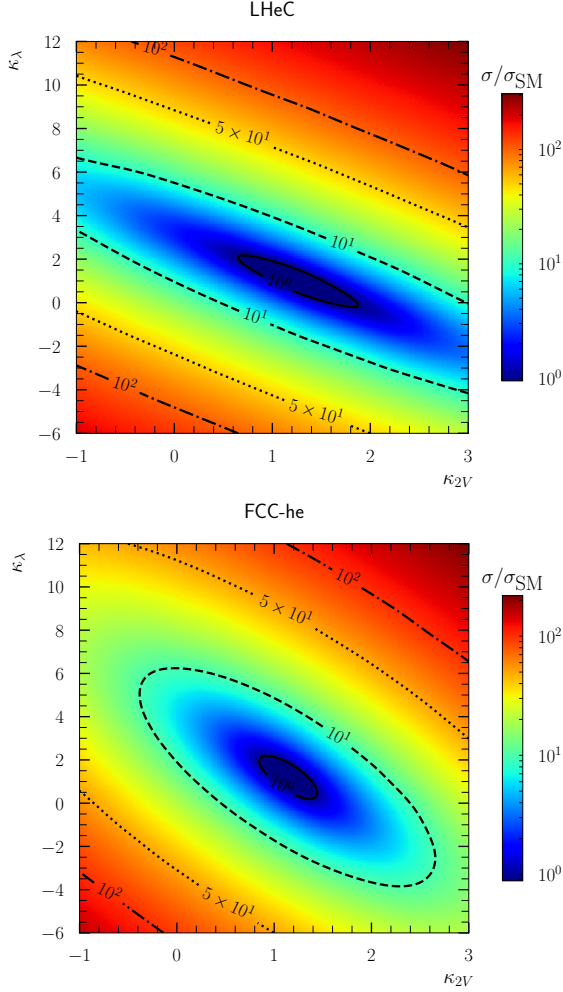


Figure 1: $\sigma/\sigma_{\text{SM}}(pe^- \rightarrow HHj\nu_e)$ projected on the plane of $(\kappa_{2V}, \kappa_\lambda)$ at the LHeC (upper panel) and FCC-he (lower panel). The SM cross-section ($\kappa_{2V} = \kappa_\lambda = 1$) with the unpolarized electron beam is $\sigma_{\text{SM}} = 5.97$ ab at the LHeC and $\sigma_{\text{SM}} = 233.77$ ab at the FCC-he.

of the contours. As shall be demonstrated, the LHeC is more sensitive to κ_λ than to κ_{2V} . The FCC-he has enough sensitivity to probe both.

For the $b\bar{b}b\bar{b}$ decay mode, the final state of the signal comprises at least four b -tagged jets, one light untagged jet, and large missing transverse energy (E_T^{miss}). The main backgrounds⁴ are the QCD multi-jets, diboson, $t\bar{t}$, and single Higgs processes, all of which are associated with a forward jet j_f and an electron neutrino ν_e . In Table 1, we show the calculation of the LO cross-sections for the backgrounds at parton level using MadGraph_aMC@NLO [38] with NNPDF31_lo parton distribution function (PDF) set [39]. Basic generator-level cuts were imposed on the parton-level objects like $p_T^j > 5$ GeV, $\Delta R_j > 0.4$, and $|\eta_j| < 10$. The renormalization and factorization scales are set to be

$$\mu_{R,0} = \mu_{F,0} \equiv \frac{1}{2} \sum_i \sqrt{p_{T,i}^2 + m_i^2}. \quad (6)$$

⁴We do not present the NC backgrounds here since they are to be highly suppressed by appropriate selection criteria.

Process	σ_{CC} [ab]	
	LHeC	FCC-he
$b\bar{b}jj + j_f\nu_e$	1.00×10^5 $^{+57.9\%}_{-33.9\%}$	7.18×10^5 $^{+51.7\%}_{-31.6\%}$
$ZZ + j_f\nu_e$	9.37×10^2 $^{+6.95\%}_{-5.45\%}$	2.24×10^4 $^{+3.65\%}_{-3.26\%}$
$Zb\bar{b} + j_f\nu_e$	5.38×10^2 $^{+27.5\%}_{-19.9\%}$	4.77×10^3 $^{+22.6\%}_{-17.1\%}$
$ZH + j_f\nu_e$	1.23×10^2 $^{+7.29\%}_{-6.27\%}$	3.45×10^3 $^{+3.99\%}_{-3.58\%}$
$b\bar{b}b\bar{b} + j_f\nu_e$	1.82×10^2 $^{+53.8\%}_{-32.4\%}$	7.11×10^2 $^{+50.9\%}_{-31.4\%}$
$Hb\bar{b} + j_f\nu_e$	4.53×10 $^{+28.4\%}_{-20.4\%}$	4.77×10^2 $^{+23.7\%}_{-17.8\%}$
$t\bar{t} + j_f\nu_e$	2.00×10 $^{+29.6\%}_{-21.2\%}$	7.49×10^2 $^{+22.9\%}_{-17.4\%}$

Table 1: Parton level cross-sections in attobarn (ab) for the charged-current background processes at the LHeC with $E_e = 50$ GeV and $E_p = 7$ TeV and at the FCC-he with $E_e = 60$ GeV and $E_p = 50$ TeV. The electron beam is unpolarized. We have not included the decays of Z , H , and the top quark. The uncertainties correspond to scale variations around the nominal scale defined in Eq. (6). PDF uncertainties are at the percent level and hence are not shown here. SysCalc [40] was used to compute these uncertainties.

The total cross-section of all the CC backgrounds is about 100 fb (751 fb) at the LHeC (FCC-he). The most dominant is the QCD production of $b\bar{b}jj$,⁵ where j refers to a light quark (including a charm quark) or a gluon. The second dominant backgrounds are from the production of a Z boson associated with another Z boson, the QCD $b\bar{b}$, or a Higgs boson. The QCD production of four b quarks follows, and the production of a Higgs boson in association with $b\bar{b}$ is less critical. Finally, the contribution of a top quark pair production is smaller than the QCD $4b$ at the LHeC, but similar at the FCC-he. Important theoretical uncertainties arose from the scale variations, as shown in Table 1. PDF uncertainties are of order 1-2% for all the backgrounds.

We close this section by summarizing the Monte Carlo event generation procedure. Initially, events for the signal and backgrounds are generated at LO using MadGraph_aMC@NLO version 2.6.7. Parton luminosities were modeled with the NNPDF31_lo PDF set with $\alpha_s(m_Z^2) = 0.118$. Setting the direction of the proton beam as forward, we convolute the partonic cross-sections with the PDFs in the LHAPDF6 library [41]. The decays of H , Z , and the top quark are modeled with MadSpin [42]. We confirmed that various kinematic distributions from on-shell samples using MadSpin well agree with those from the off-shell samples. For the parton-showering and hadronization, we rely on Pythia6 [43] since Pythia8 does not support the LHE input in electron-proton collisions yet. To correctly model hadronization of the events, we modified the default Pythia6 setup. First, we switch off the lepton PDF by setting MSTP(11)=0. Second, we also switch off the QED initial state radiation for the electron beam by setting MSTP(61)=0. Finally, we switch off the negligible multiple-parton interactions, which

⁵In what follows, we address each background process as the one without specifying $j_f\nu_e$, for simplicity.

saves a considerable amount of computing time. We use the default PDF at the Pythia6 level, CTEQ61 [44]. Fast detector simulation was performed using Delphes version 3.4.2 [45]. To match the particle efficiencies, momentum smearing, and isolation parameters with the default values in the Concept Design Report of the LHeC [22], we have performed minor modifications on the Delphes cards in the GitHub repository <https://github.com/delphes/delphes/tree/master/cards>. Jets are clustered using the anti- k_T algorithm [46] with a jet radius $R = 0.4$ in FastJet version 3.3.2 [47]. The b -tagging efficiency is set to be 70%. For the mistagging rates of the light and charm jets as a b jet, we adopted the default values in the above Delphes cards: at the LHeC, $P_{j \rightarrow b} = 0.001$ and $P_{c \rightarrow b} = 0.05$; at the FCC-he, $P_{j \rightarrow b} = 0.001$ and $P_{c \rightarrow b} = 0.04$ for $|\eta| < 2.5$, $P_{j \rightarrow b} = 0.00075$ and $P_{c \rightarrow b} = 0.03$ for $2.5 < |\eta| < 4$.

3. Results and Discussion

3.1. Event selection

In this section, we update the ATLAS analysis strategy for the VBF production of HH [16], to optimize the signal significance at the LHeC and FCC-he. As summarized in Table 2, the event selections take the following steps:

- *Initial:*
The initial number of events, n_0 , is obtained from the full detector-level simulation. We consider the decays of $H \rightarrow b\bar{b}$, $Z \rightarrow b\bar{b}$, and both the semi-leptonic and hadronic decays of a top quark pair.
- *4b-tag:*
We require the presence of at least four b -tagged jets with $p_T^b > 20$ GeV and $|\eta^b| < 5$. The acceptance times efficiency for the signal processes is around 10-16%, depending on the values of κ_λ and κ_{2V} .
- *Forward jet:*
We demand that at least one jet, untagged as a b jet, has $p_T^{j_f} > 20$ GeV and $1.5 < \eta^{j_f} < 7$. Note that the definition of being forward at asymmetric e^-p colliders is different from that at the LHC. This selection reduces the signal events by about 20%, irrespective of the hypothesis of κ_{2V} and κ_λ .
- *Lepton veto:*
We veto the events which contains an isolated lepton ($\ell = e^\pm, \mu^\pm$) with $p_T^\ell > 10$ GeV and $|\eta^\ell| < 5$. The criteria of *lepton isolation* is required so that charged leptons from heavy hadron decays are not subject to this selection but their momenta are added to the hadronic jet if $\Delta R(\ell, \text{jet}) < 0.2$. Here $\Delta R \equiv \sqrt{\Delta\eta^2 + \Delta\phi^2}$. This selection is very effective in suppressing the NC backgrounds. The event yields for the signal and CC backgrounds remain almost the same.
- *E_T^{miss} -cut:*
This selection consists of two requirements, $E_T^{\text{miss}} > 40$ GeV and $|\phi_{j_f} - \phi_{E_T^{\text{miss}}}| > 0.4$. The latter removes

the backgrounds with incorrectly measured E_T^{miss} . At this stage, the signal event yield is reduced by about 10%.

- *Minimum D_{HH} :*

The mission here is to find two Higgs boson candidates from four b -tagged jets. There are three possible combinations for pairing two b -jets out of four, called the dijet. In each combination, we order two dijets according to their transverse momentum, and call them the ‘leading’ dijet and the ‘sub-leading’ dijet. Computing the angular separation of two b -jets inside each dijet system, ΔR_{lead} and ΔR_{slead} , we require

$$\Delta R_{\text{lead}} < \begin{cases} \frac{653 \text{ GeV}}{M_{4b}} + 0.475 & \text{if } M_{4b} < 1250 \text{ GeV,} \\ 1.0 & \text{if } M_{4b} > 1250 \text{ GeV,} \end{cases} \quad (7)$$

$$\Delta R_{\text{slead}} < \begin{cases} \frac{875 \text{ GeV}}{M_{4b}} + 0.35 & \text{if } M_{4b} < 1250 \text{ GeV,} \\ 1.0 & \text{if } M_{4b} > 1250 \text{ GeV,} \end{cases}$$

where M_{4b} is the invariant mass of the four b -tagged jets. Among the pairings that satisfy Eq. (7), we choose the pairing with the smallest value of D_{HH} as the final HH candidate. Here D_{HH} is [16]

$$D_{HH} = \sqrt{(M_{\text{dijet}}^{\text{lead}})^2 + (M_{\text{dijet}}^{\text{slead}})^2} \times \left| \sin \left(\tan^{-1} \frac{M_{\text{dijet}}^{\text{slead}}}{M_{\text{dijet}}^{\text{lead}}} - \tan^{-1} \frac{116.5 \text{ GeV}}{123.7 \text{ GeV}} \right) \right|, \quad (8)$$

where $M_{\text{dijet}}^{\text{lead}}$ ($M_{\text{dijet}}^{\text{slead}}$) is the invariant mass of the leading (sub-leading) dijet system. The values of 116.5 GeV and 123.7 GeV are adopted to properly treat the energy loss in the semi-leptonic decays of the b -hadrons.

- *X_{HH} -cut:*

Finally, the signal region is defined by the following variable [16]:

$$X_{HH} \equiv \sqrt{\left(\frac{M_{\text{dijet}}^{\text{lead}} - 123.7 \text{ GeV}}{11.6 \text{ GeV}} \right)^2 + \left(\frac{M_{\text{dijet}}^{\text{slead}} - 116.5 \text{ GeV}}{18.1 \text{ GeV}} \right)^2}. \quad (9)$$

The ATLAS collaboration required $X_{HH} < 1.6$ to maximize the LHC signal significance. To optimize the search at the LHeC and FCC-he, we present the differential cross-sections as a function of X_{HH} for the LHeC and FCC-he in Fig. 2. The histograms in gray represent the total background distributions. We also show the signal results in six different hypotheses of $(\kappa_\lambda, \kappa_{2V}) = \{(-6, -1), (12, 3), (0, 3), (1, 1), (-3, 0), (5, 0)\}$ in green, blue, olive, red, purple, and cyan respectively. It is clear to see that the backgrounds are distributed in the high X_{HH} region. We have calculated the signal significance, to be defined below, for different values of the upper-cut on X_{HH} . We found that $X_{HH} < 3$ ($X_{HH} < 2$) at the LHeC (FCC-he) maximizes the signal significance, by which we

Cut	$b\bar{b}jj/b\bar{b}b\bar{b}$	ZZ/HZ	$(Z/H)b\bar{b}$	$t\bar{t}$	total backgrounds	Signal ($\kappa_\lambda = \kappa_{2V} = 1$)
LHeC with $\mathcal{L}_{\text{tot}} = 1 \text{ ab}^{-1}$						
Initial	100167.05	32.10	107.41	17.65	100324.21 (100%)	1.98 (100%)
4 <i>b</i> -tag	4.36	2.77	2.26	0.02	9.41 (0.0094%)	0.25 (12.34%)
Forward jet	1.80	2.15	1.24	0.01	5.20 (0.0052%)	0.17 (8.88%)
Lepton veto	1.80	2.15	1.24	0.01	5.20 (0.0052%)	0.17 (8.88%)
$E_T^{\text{miss}} > 40 \text{ GeV}$	1.33	1.52	0.95	0.01	3.81 (0.0038%)	0.074 (3.73%)
Minimum D_{HH}	1.27	1.48	0.91	0.01	3.66 (0.0037%)	0.064 (3.25%)
$X_{HH} < 3.0$	0.15	0.23	0.17	0.00	0.55 (0.00043%)	0.04 (2.04%)
FCC-he with $\mathcal{L}_{\text{tot}} = 10 \text{ ab}^{-1}$						
Initial	7180161	8141.8	9989.6	6673.6	7204970.0 (100%)	779.70 (100%)
4 <i>b</i> -tag	934.2	745.6	274.7	24.2	1978.7 (0.026%)	94.05 (12.06%)
Forward jet	562.6	637.1	185.6	21.9	1407.2 (0.018%)	74.71 (9.58%)
Lepton veto	562.5	637.0	185.6	18.8	1403.9 (0.018%)	74.71 (9.58%)
$E_T^{\text{miss}} > 40 \text{ GeV}$	492.3	497.7	153.0	16.2	1159.2 (0.015%)	42.11 (5.40%)
Minimum D_{HH}	412.9	458.8	129.9	13.9	1015.5 (0.014%)	29.71 (3.81%)
$X_{HH} < 2.0$	29.8	32.6	10.2	1.5	74.1 (0.00098%)	10.99 (1.41%)

Table 2: Cut-flow chart of the number of events of the signal and backgrounds at the LHeC and the FCC-he with the unpolarized electron beam. The background processes are denoted as omitting $j_l \nu_e$ for simplicity. The numbers inside the parentheses show the acceptance times efficiency after the selection step i with respect to the initial number of events n_0 , i.e. $\epsilon_i = n_i/n_0$.

define the signal region. Note that especially at the LHeC, $X_{HH} < 3$ allows significantly more data in the signal region than the LHC cut of $X_{HH} < 1.6$, which partially offsets the weakness of the LHeC's having tiny signal events.

3.2. Results

In this section, we discuss the results of our analysis. After the full selection, the signal efficiency is about 2.0% for the LHeC and about 1.4% at the FCC-he, while the background efficiency is about $\mathcal{O}(10^{-4}-10^{-3})\%$ (see Table 2). To obtain the discovery potential, we compute the signal significance including the background uncertainty [48], defined by

$$\mathcal{S} = \left[2(N_s + N_b) \log \left(\frac{(N_s + N_b)(N_b + \delta_b^2)}{N_b^2 + (N_s + N_b)\delta_b^2} \right) - \frac{2N_b^2}{\delta_b^2} \log \left(1 + \frac{\delta_b^2 N_s}{N_b(N_b + \delta_b^2)} \right) \right]^{1/2}, \quad (10)$$

where N_s is the number of signal events, N_b is the number of background events, and $\delta_b = \Delta_{\text{bg}} N_b$ is the uncertainty in the background yields. The numbers of the signal and background events are

$$\begin{aligned} N_s &= \mathcal{L}_{\text{tot}} \times \epsilon_{HH} \sigma_{HH} \mathcal{B}_{H \rightarrow b\bar{b}}^2, \\ N_b &= \mathcal{L}_{\text{tot}} \times \left[\epsilon_{bbjj} \sigma_{bbjj} + \epsilon_{ZZ} \sigma_{ZZ} \mathcal{B}_{Z \rightarrow b\bar{b}}^2 + \epsilon_{Hb\bar{b}} \sigma_{Hb\bar{b}} \mathcal{B}_{H \rightarrow b\bar{b}} \right. \\ &\quad + 2\epsilon_{HZ} \sigma_{HZ} \mathcal{B}_{H \rightarrow b\bar{b}} \mathcal{B}_{Z \rightarrow b\bar{b}} + \epsilon_{Zb\bar{b}} \sigma_{Zb\bar{b}} \mathcal{B}_{Z \rightarrow b\bar{b}} \\ &\quad \left. + \epsilon_{t\bar{t}} \sigma_{t\bar{t}} \mathcal{B}_{t \rightarrow bjj} + 2\epsilon_{t\bar{t}} \sigma_{t\bar{t}} \mathcal{B}_{t \rightarrow bjj} \mathcal{B}_{t \rightarrow b\nu} \right], \end{aligned} \quad (11)$$

where \mathcal{L}_{tot} is the total integrated luminosity, ϵ_X is the acceptance times efficiency for the process X in the signal region,

and \mathcal{B}_X is the branching ratio of the decay X . Brief comments on the error estimation for the backgrounds are in order here. In principle, the background errors show different variation according to jet energy scale, the momentum smearing, b -tagging efficiency, jet energy resolution, and theoretical uncertainties. Since the detailed study is beyond the scope of this work, we take two simple cases, $\Delta_{\text{bg}} = 10\%$ and $\Delta_{\text{bg}} = 50\%$.⁶

In Fig. 3, we display the expected exclusions on the plane of κ_{2V} and κ_λ at the LHeC (upper panel) and the FCC-he (lower panel), corresponding to $\mathcal{S} > 2$. We consider the electron beam polarization of $P_e = -80\%$ and two cases of the background uncertainty, $\Delta_{\text{bg}} = 10\%$ (solid) and $\Delta_{\text{bg}} = 50\%$ (dashed). For the total integrated luminosity \mathcal{L}_{tot} , we take 1 ab^{-1} (olive) and 10 ab^{-1} (orchid) at the LHeC, and 0.1 ab^{-1} (olive), 1 ab^{-1} (orchid), and 10 ab^{-1} (blue) at the FCC-he. The common result of the LHeC and FCC-he is that the same-sign κ_{2V} and κ_λ region is more strongly constrained because of the constructive interference discussed before.

In detail, the LHeC and FCC-he have different exclusion potential. In general, the LHeC has limitations in constraining κ_{2V} and κ_λ because of its lower center-of-mass energy. Nevertheless, it can produce some meaningful results. If $\kappa_{2V} = 1$, the LHeC data with $\mathcal{L}_{\text{tot}} = 1 \text{ ab}^{-1}$ and $\Delta_{\text{bg}} = 10\%$ can constrain κ_λ as $-3 \lesssim \kappa_\lambda \lesssim 6$, which is weaker than the HL-LHC prospect. If $\kappa_\lambda = 1$, the LHeC data with $\mathcal{L}_{\text{tot}} = 1 \text{ ab}^{-1}$ and $\Delta_{\text{bg}} = 10\%$ can exclude $\kappa_{2V} \lesssim -1$ and $\kappa_{2V} \gtrsim 3.2$, which is compatible with the current bound on $\kappa_{2V} \in [-0.66, 2.89]$ at 95% C.L. [16].

⁶In this study, we adopted a conservative approach for the background uncertainties. Considering the expected improvement of various precisions, e.g., the PDF precision at the LHeC, we expect that $\Delta_{\text{bg}} = 10\%$ can be obtained in the future.

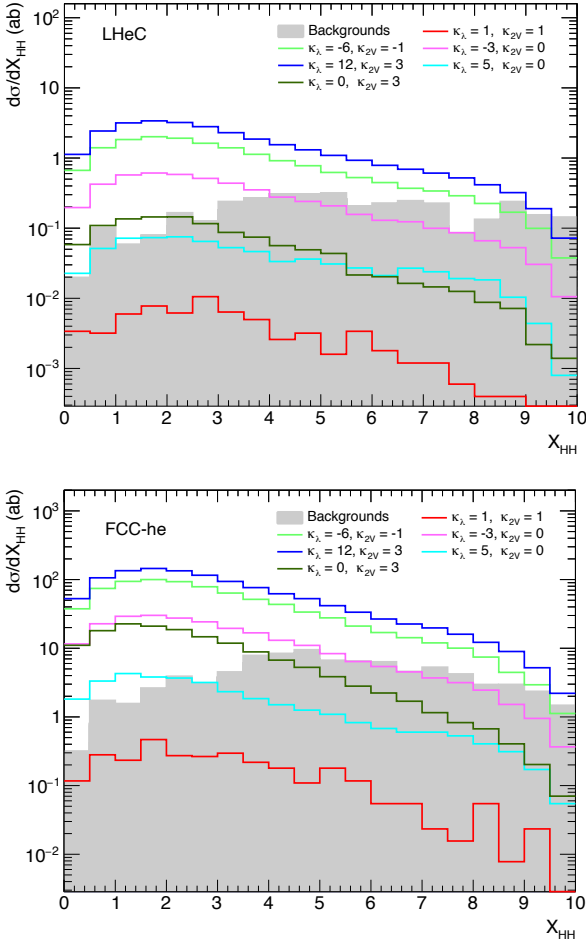


Figure 2: The differential cross-sections as a function of X_{HH} at the LHeC (upper panel) and FCC-he (lower panel) with the unpolarized electron beam. The total background is shown as the histogram in gray. The six different signal hypotheses are $(\kappa_\lambda, \kappa_{2V}) = \{(-6, -1), (12, 3), (0, 3), (1, 1), (-3, 0), (5, 0)\}$ shown in green, blue, olive, red, purple, and cyan respectively.

Considering the feasibility of the concurrent operation of the HL-LHC and LHeC, two colliders shall play a complementary role in probing κ_{2V} . In terms of the ratio of the cross-section of the CC VBF production of HH to the SM value, the LHeC with $\mathcal{L}_{\text{tot}} = 1 \text{ ab}^{-1}$ and $\Delta_{\text{bg}} = 10$ (50)% can limit $\sigma/\sigma_{\text{SM}} \lesssim 30$ (35).

On the other hand, the FCC-he has high potential in probing both κ_{2V} and κ_λ . For $\kappa_\lambda \in [0.1, 2.3]$ suggested by the HL-LHC prospect study [3], $|\kappa_{2V}| \gtrsim 0.2$ is to be excluded by the FCC-he data with $\mathcal{L}_{\text{tot}} = 10 \text{ ab}^{-1}$ and $\Delta_{\text{bg}} = 10\%$. Two important reasons for this high precision are higher signal cross-section and similar rejection rates of the SM backgrounds (see Table 2). At the FCC-he with $\Delta_{\text{bg}} = 10\%$ (50%), we estimated conservative bounds on the ratio of the Higgs pair production cross section to the SM value as follows:

$$\frac{\sigma}{\sigma_{\text{SM}}}\Big|_{\text{FCC-he}} < \begin{cases} 11 \text{ (14)} & \text{for } \mathcal{L}_{\text{tot}} = 0.1 \text{ ab}^{-1}, \\ 3.5 \text{ (8)} & \text{for } \mathcal{L}_{\text{tot}} = 1 \text{ ab}^{-1}, \\ 1 \text{ (7)} & \text{for } \mathcal{L}_{\text{tot}} = 10 \text{ ab}^{-1}. \end{cases} \quad (12)$$

Final comments on the role of higher electron beam energy in probing the HH process are in order here. Although it is practi-

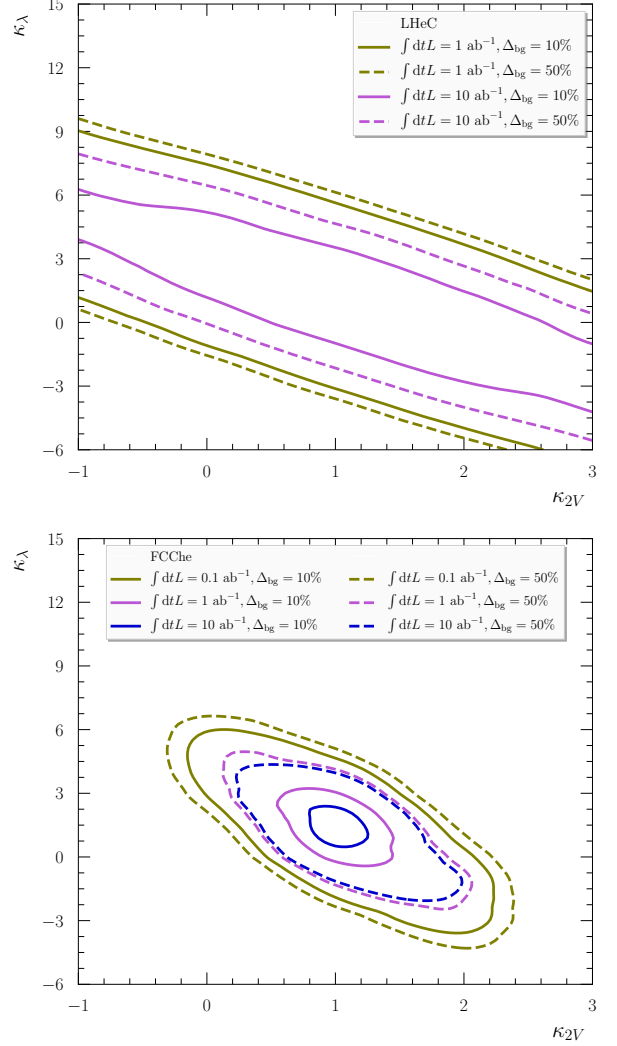


Figure 3: The expected exclusions from Higgs boson pair production projected on $(\kappa_{2V}, \kappa_\lambda)$ at the LHeC and FCC-he with the electron beam polarization of $P_e = -80\%$. We consider several options for the total integrated luminosity: 1 ab^{-1} (olive) and 10 ab^{-1} (orchid) at the LHeC; 0.1 ab^{-1} (olive), 1 ab^{-1} (orchid), and 10 ab^{-1} (blue) at the FCC-he. Two choices of the background uncertainty are considered, $\Delta_{\text{bg}} = 10\%$ (solid) and $\Delta_{\text{bg}} = 50\%$ (dashed).

cal for the LHeC working group to choose $E_e = 50 \text{ GeV}$ due to the cost issues, the physics gain from higher E_e is more important than anything else. We found that setting $E_e = 120 \text{ GeV}$ increases the background cross sections by a factor of 2.32 (1.82) at the LHeC (FCC-he). For the signal cross sections, the enhancement factor is 2.1 – 2.7 at the LHeC and 4.4 – 5.9 at the FCC-he, depending on the values of κ_λ and κ_{2V} . Assuming similar efficiencies for both the signal and backgrounds to those in Table 2, we expect that the significance increases by a factor of 1.4 – 1.8 (3.3 – 4.4) at the LHeC (FCC-he). At the FCC-he, increasing E_e into 120 GeV has almost the same effect as increasing the total luminosity tenfold. We strongly suggest that the FCC-he working group seriously consider the higher E_e option.

4. Conclusions

Upon the current status where both the trilinear Higgs self-coupling modifier (κ_λ) and the quartic coupling modifier between a Higgs boson pair and a vector boson pair (κ_{2V}) are unmeasured, we consider two electron-proton colliders, the LHeC and FCC-he, in probing κ_λ and κ_{2V} simultaneously. As a proton-proton collider, the LHC cannot avoid the gluon fusion pollution in the VBF production of a Higgs pair, which becomes much worse for $\kappa_\lambda \neq 1$. At electron-proton colliders, the gluon fusion pollution is absent, and thus the charged-current VBF production of a Higgs boson pair can be solely measured if there is enough signal significance. With this motivation, we study the detailed phenomenology of $pe^- \rightarrow HHj\nu_e$ in the $b\bar{b}b\bar{b}$ final state and suggest a search strategy at the LHeC and FCC-he based on the full simulation. Taking the default CDR values, we took $E_e = 50$ (60) GeV and $E_p = 7$ (50) TeV at the LHeC (FCC-he).

First, we calculated the parton-level cross-sections of the signal in the parameter space of $(\kappa_{2V}, \kappa_\lambda)$ as well as all relevant backgrounds. Theoretical uncertainties from the variations of the scales and PDF are also calculated. Although the backgrounds are relatively manageable, the SM cross-section ($\kappa_{2V} = \kappa_\lambda = 1$) is extremely small: without including the Higgs boson decays, $\sigma_{\text{SM}} = 5.97$ ab at the LHeC and $\sigma_{\text{SM}} = 233.77$ ab at the FCC-he for the unpolarized electron beam. It is very challenging to measure this process for the SM values of κ_λ and κ_{2V} . What is hopeful is that a small deviation from $\kappa_\lambda = \kappa_{2V} = 1$ greatly enhances the signal rate. The electron-proton collider can exclude a large portion of the $(\kappa_{2V}, \kappa_\lambda)$ space.

We have completed the analysis with full simulations to devise an optimal strategy. We found that most of the current ATLAS search strategies for HH via VBF production apply to those at the LHeC and FCC-he. The key difference of ours is the cut on X_{HH} , defined in Eq. (9). We found that the signal significance at the LHeC (FCC-he) is maximized by $X_{HH} < 3$ ($X_{HH} < 2$). A larger upper bound on X_{HH} than the one for the LHC, $X_{HH}^{\text{LHC}} < 1.6$, increases the signal significance. As the final result, we calculated the expected exclusions on $(\kappa_{2V}, \kappa_\lambda)$. The LHeC can play a meaningful role in probing κ_{2V} : the data with the total integrated luminosity of $\mathcal{L}_{\text{tot}} = 1$ ab $^{-1}$ and the background uncertainty of $\Delta_{\text{bg}} = 10\%$ can constrain $-1 \lesssim \kappa_{2V} \lesssim 3.2$ for $\kappa_\lambda = 1$. The FCC-he has immense power in constraining both κ_{2V} and κ_λ . If $\kappa_\lambda \in [0.1, 2.3]$ as the HL-LHC prospect, $|\kappa_{2V}| \gtrsim 0.2$ is to be excluded with $\mathcal{L}_{\text{tot}} = 10$ ab $^{-1}$ and $\Delta_{\text{bg}} = 10\%$. We hope that this study would provide input to strongly support the future programs of electron-proton colliders which are capable of measuring two fundamental couplings, κ_{2V} and κ_λ .

Acknowledgments

The authors would like to thank Mukesh Kumar and Xifeng Ruan for stimulating discussions and for providing the necessary material to reproduce their results. AJ would like to thank Oliver Fischer for pointing out to the updated Delphes cards for the LHeC and FCC-he. This work is supported by

the National Research Foundation of Korea, Grant No. NRF-2019R1A2C1009419.

References

- [1] G. Aad, et al., Combined measurements of Higgs boson production and decay using up to 80 fb $^{-1}$ of proton-proton collision data at $\sqrt{s} = 13$ TeV collected with the ATLAS experiment, Phys. Rev. D 101 (1) (2020) 012002. arXiv:1909.02845, doi:10.1103/PhysRevD.101.012002.
- [2] Combined Higgs boson production and decay measurements with up to 137 fb $^{-1}$ of proton-proton collision data at $\sqrt{s} = 13$ TeV.
- [3] M. Cepeda, et al., Report from Working Group 2: Higgs Physics at the HL-LHC and HE-LHC, CERN Yellow Rep. Monogr. 7 (2019) 221–584. arXiv:1902.00134, doi:10.23731/CYRM-sb2019-sb007.221.
- [4] K. Cheung, A. Jueid, C.-T. Lu, J. Song, Y. W. Yoon, Disentangling new physics effects on nonresonant Higgs boson pair production from gluon fusion, Phys. Rev. D 103 (1) (2021) 015019. arXiv:2003.11043, doi:10.1103/PhysRevD.103.015019.
- [5] G. Aad, et al., Combination of searches for Higgs boson pairs in pp collisions at $\sqrt{s} = 13$ TeV with the ATLAS detector, Phys. Lett. B 800 (2020) 135103. arXiv:1906.02025, doi:10.1016/j.physletb.2019.135103.
- [6] A. M. Sirunyan, et al., Combination of searches for Higgs boson pair production in proton-proton collisions at $\sqrt{s} = 13$ TeV, Phys. Rev. Lett. 122 (12) (2019) 121803. arXiv:1811.09689, doi:10.1103/PhysRevLett.122.121803.
- [7] A. Adhikary, S. Banerjee, R. K. Barman, B. Bhattacharjee, S. Niyogi, Revisiting the non-resonant Higgs pair production at the HL-LHC, JHEP 07 (2018) 116. arXiv:1712.05346, doi:10.1007/JHEP07(2018)116.
- [8] J. Chang, K. Cheung, J. S. Lee, C.-T. Lu, J. Park, Higgs-boson-pair production ($H \rightarrow b\bar{b}H \rightarrow \gamma\gamma$) from gluon fusion at the HL-LHC and HL-100 TeV hadron collider, Phys. Rev. D 100 (9) (2019) 096001. arXiv:1804.07130, doi:10.1103/PhysRevD.100.096001.
- [9] S. Homiller, P. Meade, Measurement of the Triple Higgs Coupling at a HE-LHC, JHEP 03 (2019) 055. arXiv:1811.02572, doi:10.1007/JHEP03(2019)055.
- [10] R. Li, X.-M. Shen, B.-W. Wang, K. Wang, G. Zhu, Probing the trilinear Higgs boson self-coupling via single Higgs production at the LHeC, Phys. Rev. D 101 (7) (2020) 075036. arXiv:1910.09424, doi:10.1103/PhysRevD.101.075036.
- [11] J. Park, J. Chang, K. Cheung, J. S. Lee, Measuring the trilinear Higgs boson self-coupling at the 100 TeV hadron collider via multivariate analysis, Phys. Rev. D 102 (7) (2020) 073002. arXiv:2003.12281, doi:10.1103/PhysRevD.102.073002.
- [12] M. L. Mangano, G. Ortona, M. Selvaggi, Measuring the Higgs self-coupling via Higgs-pair production at a 100 TeV p-p collider, Eur. Phys. J. C 80 (11) (2020) 1030. arXiv:2004.03505, doi:10.1140/epjc/s10052-sb020-sb08595-sb3.
- [13] J. Amacker, et al., Higgs self-coupling measurements using deep learning in the $b\bar{b}b\bar{b}$ final state, JHEP 12 (2020) 115. arXiv:2004.04240, doi:10.1007/JHEP12(2020)115.
- [14] M. Abdughani, D. Wang, L. Wu, J. M. Yang, J. Zhao, Probing triple Higgs coupling with machine learning at the LHC arXiv:2005.11086.
- [15] F. A. Dreyer, A. Karlberg, Vector-Boson Fusion Higgs Pair Production at N 3 LO, Phys. Rev. D 98 (11) (2018) 114016. arXiv:1811.07906, doi:10.1103/PhysRevD.98.114016.
- [16] G. Aad, et al., Search for the $HH \rightarrow b\bar{b}b\bar{b}$ process via vector-boson fusion production using proton-proton collisions at $\sqrt{s} = 13$ TeV with the ATLAS detector, JHEP 07 (2020) 108. arXiv:2001.05178, doi:10.1007/JHEP07(2020)108.
- [17] M. J. Dolan, C. Englert, N. Greiner, K. Nordstrom, M. Spannowsky, $hhjj$ production at the LHC, Eur. Phys. J. C 75 (8) (2015) 387. arXiv:1506.08008, doi:10.1140/epjc/s10052-sb015-sb3622-sb3.
- [18] M. J. Dolan, C. Englert, N. Greiner, M. Spannowsky, Further on up the road: $hhjj$ production at the LHC, Phys. Rev. Lett. 112 (2014) 101802. arXiv:1310.1084, doi:10.1103/PhysRevLett.112.101802.
- [19] J. Baglio, A. Djouadi, R. Gröber, M. M. Mühlleitner, J. Quevillon, M. Spira, The measurement of the Higgs self-coupling at the LHC: theoretical status, JHEP 04 (2013) 151. arXiv:1212.5581, doi:10.1007/JHEP04(2013)151.

- [20] J. L. Abelleira Fernandez, et al., A Large Hadron Electron Collider at CERN: Report on the Physics and Design Concepts for Machine and Detector, *J. Phys. G* 39 (2012) 075001. [arXiv:1206.2913](#), doi: 10.1088/0954-s β 3899/39/7/075001.
- [21] O. Bruening, M. Klein, The Large Hadron Electron Collider, *Mod. Phys. Lett. A* 28 (16) (2013) 1330011. [arXiv:1305.2090](#), doi:10.1142/S0217732313300115.
- [22] P. Agostini, et al., The Large Hadron-Electron Collider at the HL-LHC [arXiv:2007.14491](#).
- [23] A. Abada, et al., FCC Physics Opportunities: Future Circular Collider Conceptual Design Report Volume 1, *Eur. Phys. J. C* 79 (6) (2019) 474. doi:10.1140/epjc/s10052-s β 019-s β 6904-s β 3.
- [24] M. Kumar, X. Ruan, R. Islam, A. S. Cornell, M. Klein, U. Klein, B. Melhado, Probing anomalous couplings using di-Higgs production in electron-proton collisions, *Phys. Lett. B* 764 (2017) 247–253. [arXiv:1509.04016](#), doi:10.1016/j.physletb.2016.11.039.
- [25] S. Kuday, H. Saygin, I. Hoş, F. Çetin, Projections for Neutral Di-Boson and Di-Higgs Interactions at FCC-he Collider, *Nucl. Phys. B* 932 (2018) 1–14. [arXiv:1702.00185](#), doi:10.1016/j.nuclphysb.2018.05.002.
- [26] T. Appelquist, C. W. Bernard, Strongly Interacting Higgs Bosons, *Phys. Rev. D* 22 (1980) 200. doi:10.1103/PhysRevD.22.200.
- [27] A. C. Longhitano, Heavy Higgs Bosons in the Weinberg-Salam Model, *Phys. Rev. D* 22 (1980) 1166. doi:10.1103/PhysRevD.22.1166.
- [28] A. Dobado, M. J. Herrero, Phenomenological Lagrangian Approach to the Symmetry Breaking Sector of the Standard Model, *Phys. Lett. B* 228 (1989) 495–502. doi:10.1016/0370-s β 2693(89)90981-s β 7.
- [29] A. Dobado, D. Espriu, M. J. Herrero, Chiral Lagrangians as a tool to probe the symmetry breaking sector of the SM at LEP, *Phys. Lett. B* 255 (1991) 405–414. doi:10.1016/0370-s β 2693(91)90786-s β P.
- [30] M. J. Herrero, E. Ruiz Morales, The Electroweak chiral Lagrangian for the Standard Model with a heavy Higgs, *Nucl. Phys. B* 418 (1994) 431–455. [arXiv:hep-s \$\beta\$ ph/9308276](#), doi:10.1016/0550-s β 3213(94)90525-s β 8.
- [31] W. Hollik, S. Penaranda, Yukawa coupling quantum corrections to the selfcouplings of the lightest MSSM Higgs boson, *Eur. Phys. J. C* 23 (2002) 163–172. [arXiv:hep-s \$\beta\$ ph/0108245](#), doi:10.1007/s100520100862.
- [32] S. Kanemura, Y. Okada, E. Senaha, C. P. Yuan, Higgs coupling constants as a probe of new physics, *Phys. Rev. D* 70 (2004) 115002. [arXiv:hep-s \$\beta\$ ph/0408364](#), doi:10.1103/PhysRevD.70.115002.
- [33] D. T. Nhung, M. Muhlleitner, J. Streicher, K. Walz, Higher Order Corrections to the Trilinear Higgs Self-Couplings in the Real NMSSM, *JHEP* 11 (2013) 181. [arXiv:1306.3926](#), doi:10.1007/JHEP11(2013)181.
- [34] A. Arhrib, R. Benbrik, J. El Falaki, A. Jueid, Radiative corrections to the Triple Higgs Coupling in the Inert Higgs Doublet Model, *JHEP* 12 (2015) 007. [arXiv:1507.03630](#), doi:10.1007/JHEP12(2015)007.
- [35] J. Braathen, S. Kanemura, On two-loop corrections to the Higgs trilinear coupling in models with extended scalar sectors, *Phys. Lett. B* 796 (2019) 38–46. [arXiv:1903.05417](#), doi:10.1016/j.physletb.2019.07.021.
- [36] E. Arganda, C. Garcia-Garcia, M. J. Herrero, Probing the Higgs self-coupling through double Higgs production in vector boson scattering at the LHC, *Nucl. Phys. B* 945 (2019) 114687. [arXiv:1807.09736](#), doi:10.1016/j.nuclphysb.2019.114687.
- [37] C. Degrande, C. Duhr, B. Fuks, D. Grellscheid, O. Mattelaer, T. Reiter, UFO - The Universal FeynRules Output, *Comput. Phys. Commun.* 183 (2012) 1201–1214. [arXiv:1108.2040](#), doi:10.1016/j.cpc.2012.01.022.
- [38] J. Alwall, R. Frederix, S. Frixione, V. Hirschi, F. Maltoni, O. Mattelaer, H. S. Shao, T. Stelzer, P. Torrielli, M. Zaro, The automated computation of tree-level and next-to-leading order differential cross sections, and their matching to parton shower simulations, *JHEP* 07 (2014) 079. [arXiv:1405.0301](#), doi:10.1007/JHEP07(2014)079.
- [39] R. D. Ball, et al., Parton distributions from high-precision collider data, *Eur. Phys. J. C* 77 (10) (2017) 663. [arXiv:1706.00428](#), doi:10.1140/epjc/s10052-s β 017-s β 5199-s β 5.
- [40] A. Kalogeropoulos, J. Alwall, The SysCalc code: A tool to derive theoretical systematic uncertainties [arXiv:1801.08401](#).
- [41] A. Buckley, J. Ferrando, S. Lloyd, K. Nordström, B. Page, M. Rüfenacht, M. Schönherr, G. Watt, LHAPDF6: parton density access in the LHC precision era, *Eur. Phys. J. C* 75 (2015) 132. [arXiv:1412.7420](#), doi:10.1140/epjc/s10052-s β 015-s β 3318-s β 8.
- [42] P. Artoisenet, R. Frederix, O. Mattelaer, R. Rietkerk, Automatic spin-entangled decays of heavy resonances in Monte Carlo simulations, *JHEP* 03 (2013) 015. [arXiv:1212.3460](#), doi:10.1007/JHEP03(2013)015.
- [43] T. Sjostrand, S. Mrenna, P. Z. Skands, PYTHIA 6.4 Physics and Manual, *JHEP* 05 (2006) 026. [arXiv:hep-s \$\beta\$ ph/0603175](#), doi:10.1088/1126-s β 6708/2006/05/026.
- [44] P. M. Nadolsky, H.-L. Lai, Q.-H. Cao, J. Huston, J. Pumplin, D. Stump, W.-K. Tung, C.-P. Yuan, Implications of CTEQ global analysis for collider observables, *Phys. Rev. D* 78 (2008) 013004. [arXiv:0802.0007](#), doi:10.1103/PhysRevD.78.013004.
- [45] J. de Favereau, C. Delaere, P. Demin, A. Giammanco, V. Lemaitre, A. Mertens, M. Selvaggi, DELPHES 3, A modular framework for fast simulation of a generic collider experiment, *JHEP* 02 (2014) 057. [arXiv:1307.6346](#), doi:10.1007/JHEP02(2014)057.
- [46] M. Cacciari, G. P. Salam, G. Soyez, The anti- k_t jet clustering algorithm, *JHEP* 04 (2008) 063. [arXiv:0802.1189](#), doi:10.1088/1126-s β 6708/2008/04/063.
- [47] M. Cacciari, G. P. Salam, G. Soyez, FastJet User Manual, *Eur. Phys. J. C* 72 (2012) 1896. [arXiv:1111.6097](#), doi:10.1140/epjc/s10052-s β 012-s β 1896-s β 2.
- [48] G. Cowan, K. Cranmer, E. Gross, O. Vitells, Asymptotic formulae for likelihood-based tests of new physics, *Eur. Phys. J. C* 71 (2011) 1554, [Erratum: *Eur.Phys.J.C* 73, 2501 (2013)]. [arXiv:1007.1727](#), doi:10.1140/epjc/s10052-s β 011-s β 1554-s β 0.